Journal of Bio- and Tribo-Corrosion (2023) 9:8
https://doi.org/10.1007/s40735-022-00729-2

Erosion–Corrosion Behaviour of ASTM A106 GR.B Carbon Steel Pipelines

Y. Reda[1] · A. Gamal[2] · R. Abdel-Karim[2] · S. M. El-Raghy[2]

Received: 16 March 2022 / Revised: 15 July 2022 / Accepted: 21 October 2022 / Published online: 1 November 2022

Abstract

Erosion–corrosion "E–C" of the ASTM A106 Gr.B carbon steel was investigatedusing self-constructed E–C setup. Well water "NWW", extracted from Noroos Gas-Wells located at Western Desert—Egypt, was used as testing electrolyte. The effect of the impingement angle, sand content and flow pressure was studied. For comparison, similar experiments were conducted using distilled water. The test results were obtained for angles of 20°, 45°, 70° and 90° using 1.5–3 g/l suspended solids (sand) and flow pressure ranging from 20, 30 and 40 psi. It was found that the greatest E–C occurred at impact angles of roughly 70° for distilled water and 90° for well water. The erosion rate increased as the sand concentration and flow pressure increased. Optical microscopy and scanning electron microscopy (SEM) were the main characteristics of the metal surface. Ploughing and metal cutting were the primary erosion mechanisms at low impact angles, according to SEM micrographs. Flattening of ridges and fractures are the major metal removal processes at high impingement angles. At impact angle 90°, the total synergism (*S*) based on E–C is calculated to be the sum of the material loss times ~ 2.3 because of pure erosion and corrosion. In addition, the erosion contribution "E" increased with increasing impingement angle. Its values were 34.61, 47.97, 56.92 and 58.3%, for impingement angles 20°, 40°, 70° and 90°, respectively. The variation in the open-circuit potential with exposure time is quite different based on the presence of chloride ions as well as a load of sand.

Keywords Erosion · Corrosion · Steel pipeline ASTM A106 Gr.B · Erosion test · SEM · Impingement angle · OCP · Wear rate

1 Introduction

Corrosion issues plague oil and gas pipelines, refineries and petrochemical facilities. Water, carbon dioxide (CO_2) and hydrogen sulphide (H_2S) are the most common causes of internal corrosion in the oil and gas sector, and microbial activity can exacerbate the problem [1]. Additionally, the corrosion rate is heavily influenced by the flow regimes of multiphase fluids. For example, high flow rates are characterized by flow-induced corrosion and erosion–corrosion (E–C), while pitting corrosion is more prevalent at low flow rates [2].

In the oil and gas production, the petroleum products' transportation is often associated with sand particles and water which unfavourably influence the pipeline [3, 4]. Sand production is apparent late in the life of assets in many applications. In these circumstances, operating personals are hesitant to introduce sand avoidance frameworks since production rates can possibly decline [5, 6]. Many operating personnel have the option of supervising sand production by creating facilities that deal with sand once it starts production. Accordingly, very low corrosively situations can be heavily affected, and highly corrosive systems can become troubling.

The pipeline industry, as well as the petroleum society, is interested in the integrity of the pipeline and the environment. Through the E–C process, the corrosion products formed on the pipeline surface in the form of an oxide film is influenced by the mechanical activity of the solid erosion process [5]. The oxide film products' removal by the mechanical activity subjects the exposed area to more

✉ Y. Reda
ysyy5@hotmail.com

[1] Canal High Institute of Engineering and Technology, Suez, Higher Technological Institute, 10th Ramadan (HTI), Cairo 11722, Egypt

[2] Department of Metallurgy, Faculty of Engineering, Cairo University, Giza 12613, Egypt

stresses and degradation. This process is complicated and affected by numerous parameters and conditions.

The general comprehension of the E–C process is that there are electrochemical and mechanical processes that can influence each other. The authors proposed different tests and models to examine the E–C process and various results have been found in many cases [6–9]. This variation occurs due to the test conditions, materials, environment as well as equipment used in the tests. Different sources discuss the sand erosion mechanism [10–15]. This section attempts to summarize the key contributions. The most ductile materials' erosion mechanism is the first way which is described as sand particles that result in ductile ploughing of the surface. The second way was that the rate of material removal and erosion mechanism governed by the impact angle, particle impact velocity and metal mechanical properties—ductility (involves scrapping or cutting) and brittleness (involves cracking and chipping) [10]. Bitter [12, 13] introduced the third way by identifying that the solids' fluid-bed transport lines undergo two violent erosion attacks. The first was caused by repetitive distortion during impact, which resulted in scattering the material, and the second was caused by the free-moving particle's cutting action. Bitter suggested that if an acute angle was used for particles cutting strike the body, some material from the surface would be scratched. The velocity and the abrasive particles' impact angle affect this scratching.

Hutchings [14] proposed that the velocity and impact angle are affected by the fluid local hydrodynamics with forces such as drag force, buoyant force and the weight affecting the particle within a confined geometry. Particles can cross fluid streamlines due to a change in the force balance caused by a change in local fluid flow, resulting in impingement and material loss [14]. Gravel packing, sand consolidation and controlled production are examples of sand management strategies that have worked. Accordingly, over the years, various erosion prediction algorithms have been created.

The potential practical application of the work, its destructive nature due to the increasing severity of conditions attributed to material deterioration in such hydro-transport system (pipelines) transports oil sands from excavation to the extraction plants, refineries and consumer-ready products to markets.

The purpose of this research is to evaluate erosion and E–C of ASTM A106 Gr.B carbon steel using two different electrolytes well water located at Western Desert—Egypt affecting Petroleum Company. The influence of the following parameters: effect of impact angle of solid particles, concentration of solid particles, and flow pressure of electrolyte medium. For comparison, some tests were conducted using distilled water. The studies were set up to see how much each of the various corrosion–erosion processes contributed to the overall net synergism.

2 Experimental Methods

2.1 Materials

ASTM A106 Gr.B steel coupons were delivered from Petrobel Company-Egypt and were used as test specimens. Tables 1 and 2 show the chemical composition and mechanical characteristics of steel coupons. All samples were cut into 20×20 mm^2 coupons and wet-grounded up to 500 silicon carbide abrasive paper. To begin the experiments, the specimens were cleaned with distilled water and then dried weighed. Two types of electrolytes (Noroos Wells Water "NWW" from West Desert—Egypt—distilled water "DW") were used during erosion and corrosion studies. The chemical analysis of the used electrolytes is shown in Table 3. For the erosion test, a self-made sandblast type erosion testing apparatus was employed, which was effective for eroding material from a test sample while being exposed to controlled conditions. Based on the impingent angle, the erosion testing apparatus was built to modify impact pressure, specimen placement, and orientation. As illustrated in Fig. 1, the

Table 1 Chemical composition of the ASTM A106 Gr.B

Element	C	Mn	Si	P	S	Ni	Cr	Cu	Fe
Wt%	0.233	0.883	0.248	0.012	0.007	0.128	0.143	0.196	Balance

Table 2 Mechanical properties of ASTM A106 Gr.B

Yield strength (MPa)	Tensile strength (MPa)	Hardness (HV)
240	415	180

Table 3 Chemical composition of distilled water and water samples taken from Noroos wells

	"Noroos" wells water (WW)	Distilled water (DW)
Total dissolved solids, TDS (mg/l)	1830	31
Salinity as chloride (mg/l)	958.5	30.7
Calcium (Ca^{2+}) (mg/l)	100	0.1
Magnesium (Mg^{2+}) (mg/l)	59	0
Total iron (Fe^{2+}) (mg/l)	40	0
Sodium (Na^{+}) (mg/l)	621	0

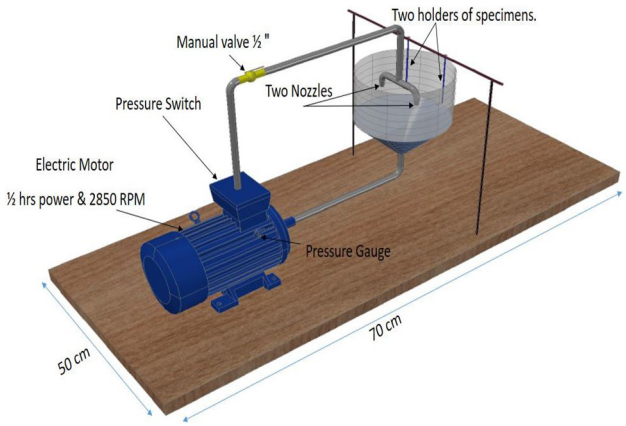

Fig. 1 Schematic view of the erosion–corrosion test setup

Table 4 Operating conditions for pure erosion and erosion–corrosion tests

Test parameter	Value
Vessel capacity	3 l
System	Closed system
Specimen	20×20 mm^2 flat coupons
The angle of impingement	20°, 45°, 70°, 90°
Nozzle diameter	5 mm
Sample distance from nozzle	5 cm
Solid loading	0, 1.5, 3 g/l
Test solution	Distilled water/well water
Test duration	4 h
Test temperature	25°
Test pressure	20, 30 and 40 psi

erosion-testing device is composed of an electrical motor, 3-l capacity water vessel, pressure gauge, pressure switch, and a specimen holder.

The double-disc technique was used to determine the particle velocity as a function of pressure. The delivery of a combination of fluid (distilled water, well water) and sand through a twin nozzle arrangement impinges on the surface of the specimen at an angle of 20°, 45°, 70° and 90°, respectively, creates a closed system. The nozzle has a diameter of 5 mm and was placed at a fixed distance of 5 cm. With a precision of 0.0001 gm, weight loss measurements were conducted using a "Sartorius balance". The test lasted 4 h, and the specimens were weighed before and afterwards (after cleaning the surface with acetone solution, distilled water and dried with compressed air to determine the total weight loss). For flow-induced corrosion testing, no solid loading was used, but 1.5 g/l and 3 g/l of sand were added to replicate erosion-corrosive conditions. Silica (SiO_2) solid particles with particle size 16 µm were used as erodent in all experiments. Table 4 summarizes the operating parameters for both pure erosion and E–C. Equation (1) shows the total E–C degradation (wt loss) in terms of volume loss (mm/h) per exposed surface (mm.^{2}) per unit time (h) [16, 17]

$$\text{Wear rate} = \frac{W}{S * \rho * t}(\text{mm}^3/\text{mm}^2\text{h}), \quad (1)$$

where W is weightloss(g), S is surfacearea$\left(\text{mm}^2\right)$, ρ is specimendensity$\left(\text{g}/\text{mm}^3\right)$, t is time(h).

2.2 Surface Morphology

Sample surface characterization related to degradation mechanism was performed by using optical microscopy OLYMPUS-Type BX41M-LED and QUANTA FEG250 Type scanning electron microscopy (SEM).

2.3 Open-Circuit Potential

During the E–C experiments, OCP measurements were taken against the silver chloride electrode reference electrode. The measurements were taken at 30-min intervals during the test.

3 Results and Discussion

3.1 Effect of Working Media

At impact angle of 90° and flow pressure of 20 psi**,** the effect of working media was studied. As illustrated in Fig. 2, the highest weight loss of the specimen was in case of using well water with sand. The wear rate values were 1.67, 2.55, 1.83 and 10.36 (mm^3/mm^2 h) for distilled water, distilled water with sand, well water and well water with sand, respectively. Due to the continued cutting wear and repetitive deformation, the weight loss of specimens increased as the severity

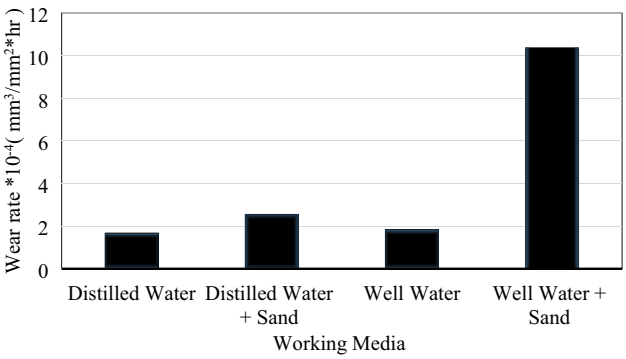

Fig. 2 Effect of working media on the wear rate of ASTM A106 Gr.B carbon steel at angle of 90° using sand content 1.5 g/l with flow pressure of 20 psi

of the working media increased. The high severity of the well water is due to the high concentration of chloride ions in the well water compared to that in the distilled water. The presence of Cl^- ion in water can accelerate the corrosion of carbon steel [18, 19] by increasing the electro-conductivity in the system [1, 20].

The working mechanism for corrosive wear caused by the impact of the suspended solids in the electrolyte medium can be elucidated as follows. First, the erosion is fluctuated because of stress hardening as well as the hardness of metal surface caused by the impact of the surface with sand. The stress-hardened surface layers will break down under the constant impact of sand. Any passivation film on the surface will be broken down repeatedly because of the influence of high-pressure jet. The Cl^- ions could immediately work on the bare surface, resulting in metal dissolution [18]. This confirms Ramakrishna Malka's [21, 22] platelet mechanism, which states that in erosion, plastic deformation occurs as a consequence of repeated hits, culminating in deformation hardening of the surface scales until they break off.

3.2 Effect of Content of Solid

At low impact angle (200), the effect of content of solid was studied. As indicated in Fig. 3, the weight loss under E–C of ASTM A106 Gr.B carbon steel in well water with sand increases with increasing sand content. The values of metal loss at 0 g, 1.5 g and 3 g sand loading were 1.35, 2.07 and 3.75 (mm^3/mm^2 h), respectively. In general, the steel in the streaming corrosive environment will dissociate, showing that oxygen reduction enhances the corrosion process. The presence of sand in a streaming corrosive environment reduces the density of the oxygen diffusive layer, hastening oxygen cathodic reduction. The intensity of the erosive to the steel electrode increases as the sand concentration rises, resulting in a more active electrode state [19].

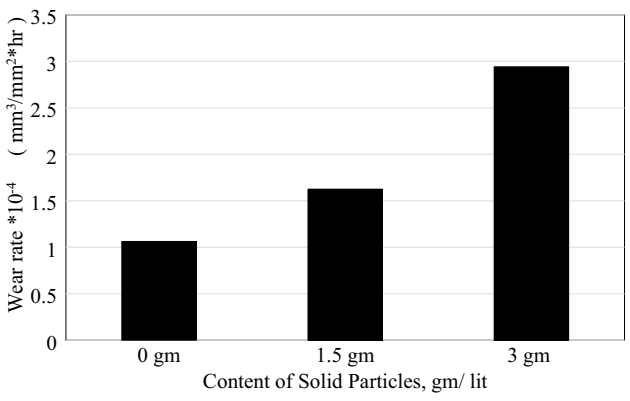

Fig. 3 Effect of solid particles content on wear rate measured using well water at impingement angle 20° for 4 h, with flow pressure 20 psi

Furthermore, the rate of erosion increases as the sand concentration rises due to the greater chance of sand particles impacting the steel surface [19, 23]. Accordingly, as the sand concentration increases, the E–C mechanism of steel flips from E–C to erosion-dominant. The SEM surface morphology of the ASTM A106 Gr.B carbon steel after 4 h of E–C test as a function of sand content is illustrated in Fig. 4. As a result of erosive particles penetrating the steel surface, a large number of affected holes with deep grooves were widely scattered on the steel surface. Surface roughness, as measured by the number and diameter of impacting holes, rose as the sand concentration increased.

3.3 Effect of the Pressure of Electrolyte

At an angle of 20°, sand content of 1.5 g/l, the effect of the pressure of electrolyte was studied. As illustrated in Fig. 5, as the electrolyte pressure was raised, the weight loss readings of ASTM A106 Gr.B carbon steel rose. The values of metal loss were 2.07, 2.77 and 3.12 (mm^3/mm^2 h) at 20, 30 and 40 psi impact pressure, respectively. Moreover, it is creating an effective area for corrosion.

Figure 6 shows a SEM of the degraded surface. At low fluid pressure, Fig. 6a the form of the eroded surface clearly has some erosive tracks, ploughing and chip formation, small pits area and some depth. That is, at minimal fluid pressure, the majority of the collision is elastic and does not affect the erosion rate. At high fluid pressure as illustrated in Fig. 6b, the form of the eroded surface has larger pits area, and the corrosion cavities are deeper with a large area. Some metal cutting can be seen; according to Islam et al. [24], silicon oxide particles strike the surface and induce heavy plastic distortion on the surface, as well as some of the particles, embedded into the matrix.

3.4 Effect of Impact Angle of Solid Particles

Using 1.5 g/l sand and flow pressure 20 psi, *the effect of impact angle of solid particles was studied*. Figures 7 and 8 illustrate the weight loss measurements of the specimen using well water with sand as a function of impingement angles. The weight loss of ASTM A106 Gr.B carbon steel increased with an increasing impact angle. The values of metal loss were 2.07, 2.31, 5.50 and 10.36 (mm^3/mm^2 h), at 20°, 45°, 70° and 90° impact angles, respectively. Based on the foregoing data, it was determined that the tested material has the maximum wear rate at an impact angle of 90°.

The wear rate of ASTM A106 Gr.B carbon steel in distilled water with sand increased with an impact angle. The values of metal loss were 0.72, 0.95, 2.94 and 2.55 (mm^3/mm^2 h), at 20°, 45°, 70° and 90° impact angles, respectively, at the same sand content of 1.5 g. At an impact angle of 70°, the tested material's wear rate was the greatest.

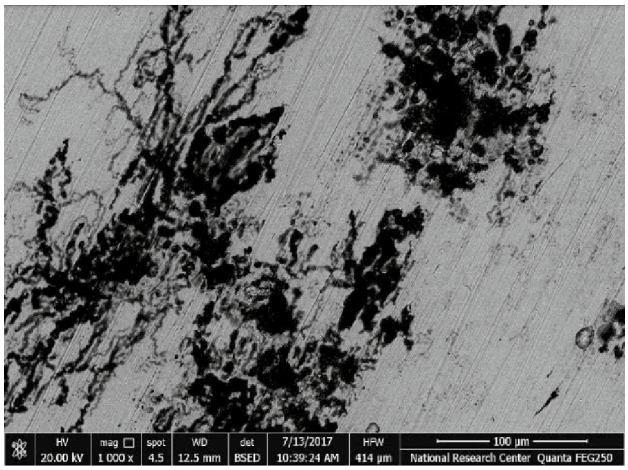

(a)

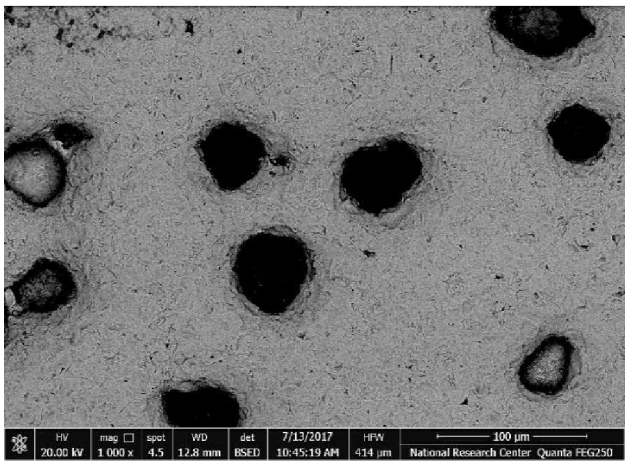

(b)

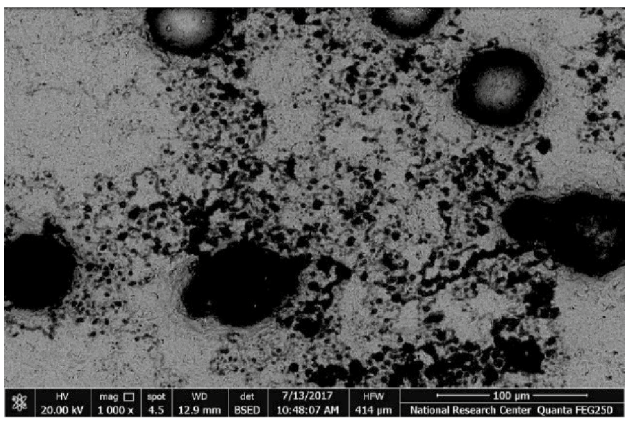

(c)

Fig. 4 SEM micrographs of ASTM A106 Gr.B carbon steel, using a well water environment, angle of 20°, at different sand content **a** 0 g sand, **b** 1.5 g sand, and **c** 3 g sand

The eroded surfaces were examined using an optical microscope and a SEM to further understand the impact angle's effect on the material elimination mechanism.

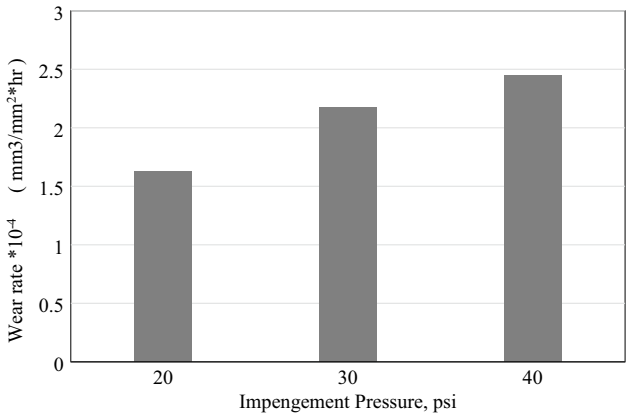

Fig. 5 Wear rate measured using well water at different electrolyte pressure at an angle of 20°, sand content of 1.5 g/l

Figure 9 illustrates the microstructure of the specimen using well water with sand using an optical microscope at impact angles of 20°, 45°, 70° and 90°, respectively. The resolved normal stress of impacted sands rose as the impact angle was raised from 20° to 45°.

This resulted in less sand sliding and increased sand penetration into the surface. As a result, shorter erosive tracks with wider elevated lips are better produced. Figure 9b in comparison with the impact angle of 20°. In case of, Fig. 9a, if the impact angle increases to 45° Fig. 9b, the direction of grooves becomes random and the amount of small holes caused by the normal stress decreases. As the impact angle continuously increases to 70°, the grooves on the surface decrease and several big holes could be observed in Fig. 9c. According to Abedini and Ghasemi [25], sliding abrasion causes mechanical erosive wear tracks in both E–C and erosion tests at a low impact angle of 20°, which could be the result of peels of the metallic surface layer (material removal) by a micro-cutting mechanism based on the oblique shear stress. Sand impact force may produce plastic deformation of the surface material, resulting in erosive tracks with enlarged surface lips. At minimum impact angles, the lower resolved normal and larger tangential components of stress induced by sands on the surface might introduce a prolonged sliding and cutting time. Following collisions might distort and eventually separate the malformed lips, causing grooves. By further increment of contact angle up to 90°, the severity of attack increased and many pits were formed. Due to the low resolved normal stress and limited penetration of impacted sands at a 20° angle, many impacts may be required to remove the material from the surface, resulting in low E–C and erosion rates. According to prior research [25–28], at a 90° impact angle, the resolved normal stress will cause cumulative damage on the surface, including raised lips, pitting, grooves, and craters surrounding the

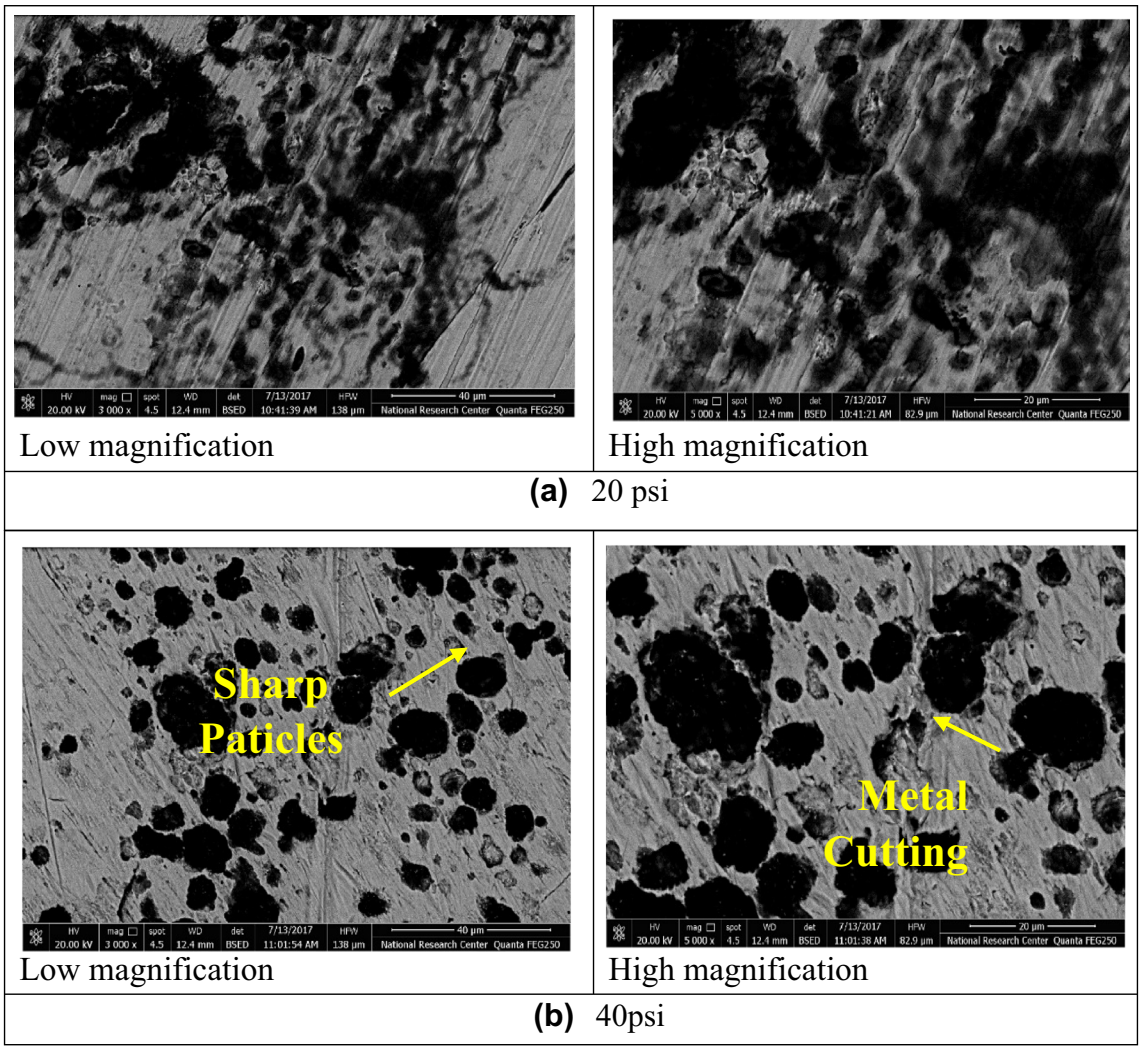

Fig. 6 SEM micrographs of ASTM A106 Gr.B steel using well water with 1.5 g sand content, at an impact angle of 20°, **a** flow pressure of 20 psi, and **b** flow pressure of 40 psi

impact zone, resulting mostly from fatigue, microforging, and throwing/extrusion processes.

Erosion rates for fragile materials increase with increasing impact angle up to 90°, according to several authors. For ductile materials, erosion rate climbs significantly with increasing impact angle, peaking between 15° and 40°, and then falling [29]. Brittle materials shatter at extreme collision angles, according to earlier research, but ductile materials show severe plastic deformation. It is possible to discern deformation scratches and lip creation caused by plastic deformation caused by extrusion action, which is consistent with the findings of other writers [30–33]. The ductile erosion behaviour of carbon steel ASTM A106 Gr.B at a 90° impact angle is characterized by dimples, pits and crater morphologies, which are common in ductile metals at typical impacts [30, 33]. On the specimen surface, there are several grooves running in the same direction (fluid impact direction), as well as an impact scar with tiny holes.

The combined effect of shear stress and normal stress acting on the metal surface might explain the change in surface shape generated by varied impact angles. The falling of the particles at a tiny impact angle might push the material towards the direction of the impact, causing a scratch on the metal surface. As a result of the oblique shear force, material is removed and plastic deformation occurs [19, 34]. The vertical incidence is nearly the primary mechanism for high impact angles, which may generally form large craters (holes) on the surface due to normal stress [19, 35]. Shear stress and normal stress are both quite tiny at the medium impact angle, and hence, the combined effect on mechanical damage is relatively weak. The findings are in line with the surface morphologies described in the literature [19].

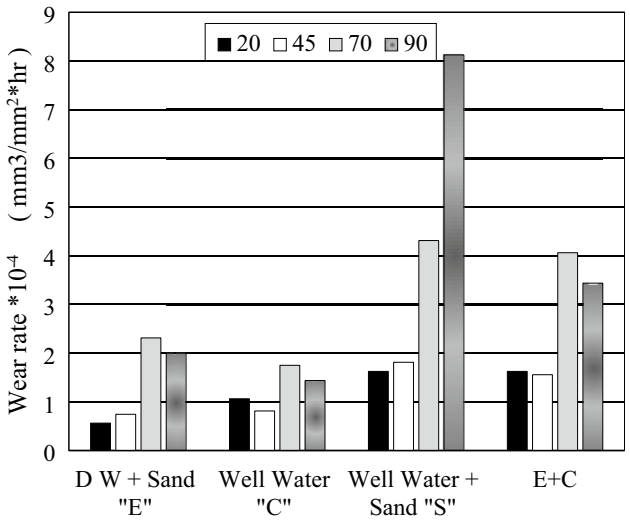

Fig. 7 Effect of impact angle of solid particles on the wear rate of ASTM A106 Gr.B and synergistic effect for 4 h using different media with 1.5 g sand content

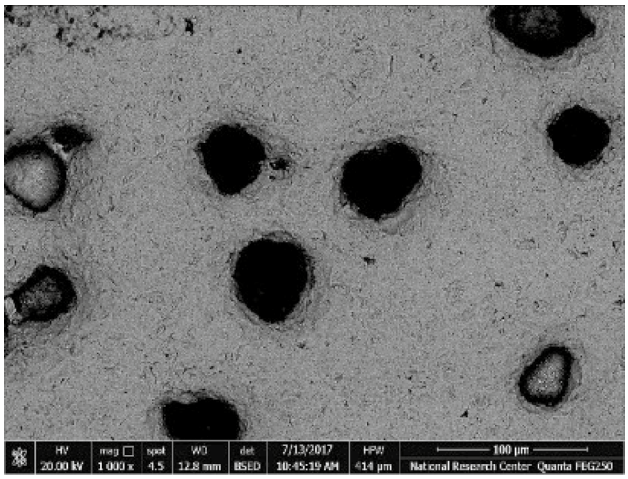

(a1) Specimen A at 1000X

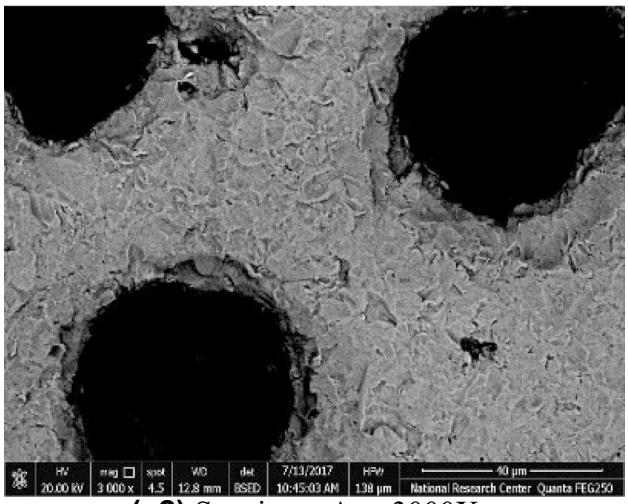

(a2) Specimen A at 3000X

Fig. 8 SEM micrographs of the specimen using well water containing 1.5 g/l sand at impact pressure 20 psi and impingement angle 90°

3.5 Effect of Synergy Between Erosion and Corrosion

A comparison of the change in weight loss due to corrosion "C" in well water, due to erosion "E" in distilled water + sand, as well as the rate of E–C in well water + sand were calculated from data presented in Fig. 7. It is clearly shown that the E–C rate is more affected by synergism. The synergistic effect "S" increased with increasing the impact angle. At impact angle of 90°, the total synergism (*S*) based on E–C conditions is calculated to be ~ 2.3 times the sum of the material loss because of pure erosion and corrosion, separately. Erosion has a major impact on corrosion because impacting solid particles break the surface and activate specific areas, speeding up corrosion damage. The percentage contribution of erosion "E" increased with increasing impingement angle. Its values were 34.61, 47.97, 56.92 and 58.3%, for impingement angles 20°, 40°, 70° and 90°, respectively.

The influence of corrosion on erosion is enormous, as seen by a comparison of pure erosion and the erosion rate component in the combined E–C process. It is thought that corrosion roughens the surface and generates flaws, causing the anodic work-hardened layer to be removed and a weakly attached passive coating to develop on the surface [36, 37]. This passive layer is easily removed during erosion by inserting the abrasive particles (increases weight loss). These embedded particles act as crevice sites for pit formation, and a fresh unhardened surface is exposed to erosion (giving rise to higher erosion rate) [38, 39]. Further, because of high particle pressure, the particle sharpness creates micro-cracks. Corrosive electrolyte reaches the subsurface region throughout the corrosion process cycle, extending these fissures. In the next erosion process cycle, this promotes separation (i.e. delamination) [40].

The drastic increase in wear rate for combination of well water and sand is due to the max concentration by weight of chloride per unit volume. The increase of sand gives roughness to the surface generate flaws causing the anodized work-hardened layer to be removed and a weakly attached passive coating developed on the surface which is easily removed during erosion leading to the increase of weight loss. The increasing of sand content in well water causes a significant surface deterioration and a remarkable shift to more negative potential value.

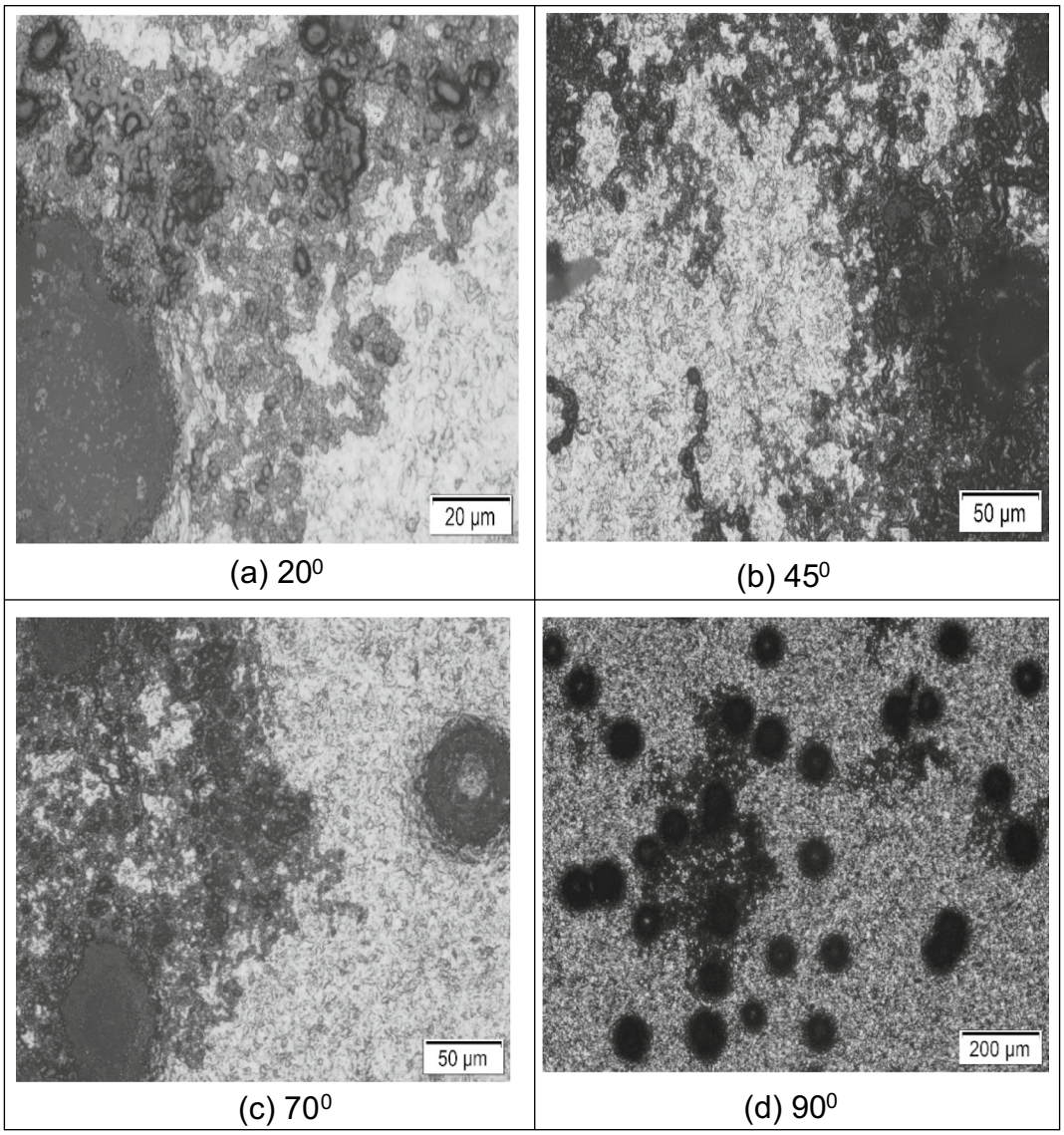

Fig. 9 The microstructure of the specimen using well water at different angles using 1.5 g/l sand **a** 20°, **b** 45°, **c** 70° and **d** 90° using an optical microscope

3.6 Open-Circuit Potential

Figure 10 illustrates the potentials of the open circuit as a function of time measured for ASTM A106 Gr.B carbon steel coupons tested in well water as well as distilled water with different sand loading and 90° impingement angle, for 4 h. The overall potential values were negatively shifted with increasing exposure time especially in the case of well water. Increasing the sand content in well water caused by significant surface deterioration and a remarkable shift in the open-circuit potential (OCP) towards more negative values. The most negative OCP was measured in case of well water with 3 g/l sand (~ − 1000 mV). Because of the significant negative change in potential, ASTM A106 Gr.B carbon steel was deemed to be in active corrosion after only a few seconds of immersion.

Meanwhile, the measured potential values of test coupons after being subjected to distilled water for 4 h were − 500 mV, − 578 mV, − 692 mV and 742 mV SSC, at 0 g, 1.5 g and3 g of sand content, respectively. In this situation, the production of corrosion products and/or an oxide coating on the surface induced a very minor shift in the potential of carbon steel over time, which offered some protection for carbon steel but did not totally prevent its dissolution [41, 42].

The above values concluded that the variation in the OCP with exposure time is quite different based on the presence of chloride ions as well as a load of sand. Increased energy transmission from the sand to the surface was seen in well

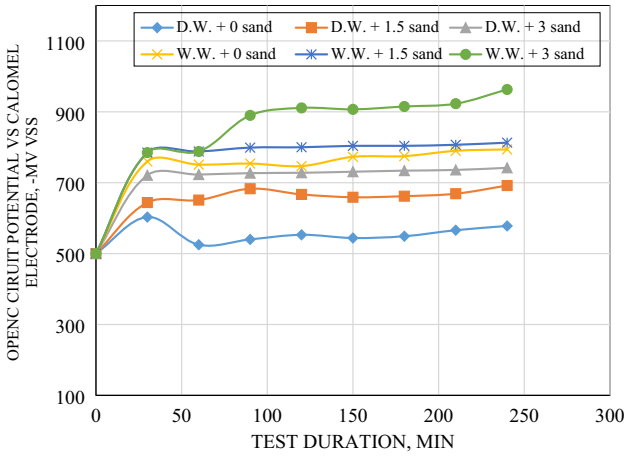

Fig. 10 Open-circuit potential of ASTM A106 Gr.B carbon steel tested in well water as well as distilled water with different sand loading content for 4 h

water and distilled water with higher sand concentration. The chloride ions in the well water attacked the created air oxide coating, forcing it to dissolve, allowing the surface-active material to emerge.

3.7 Statistical Analysis

Statistical analysis was conducted for all the factor in order to evaluate the results, the results are seen in Fig. 11. Statistical analysis shows a linear relation between wear rate and **impingement** pressure as shown in Fig. 11a, Linear relation between wear rate and content of solid particles is shown in Fig. 11b, and polynomial equation between wear rate and impact angle degree is seen in Fig. 11c.

The regression coefficient shows an equation of the first degree for both relation of wear rate with **impingement** pressure and content of solid particles, while regression coefficient shows an equation form the third degree for relation of wear rate with impact angle degree.

4 Conclusion

The highest weight loss of the specimen was observed using well sand water compared with distilled sand water. The E–C rate of ASTM A106 Gr.B carbon steel using well water increased with sand concentration. Enhance E–C rates of ASTM A106 Gr.B carbon steel were registered with a higher flow pressure of electrolyte. In the case of well water containing 1.5 g/l sand, the highest E–C rate of ASTM A106 Gr.B carbon steel was detected at an impact angle of 90°. The same trend was detected at an impact angle of 70° for distilled water containing the same content of sand. The synergism highly affects the E–C rate. Its effect increased with

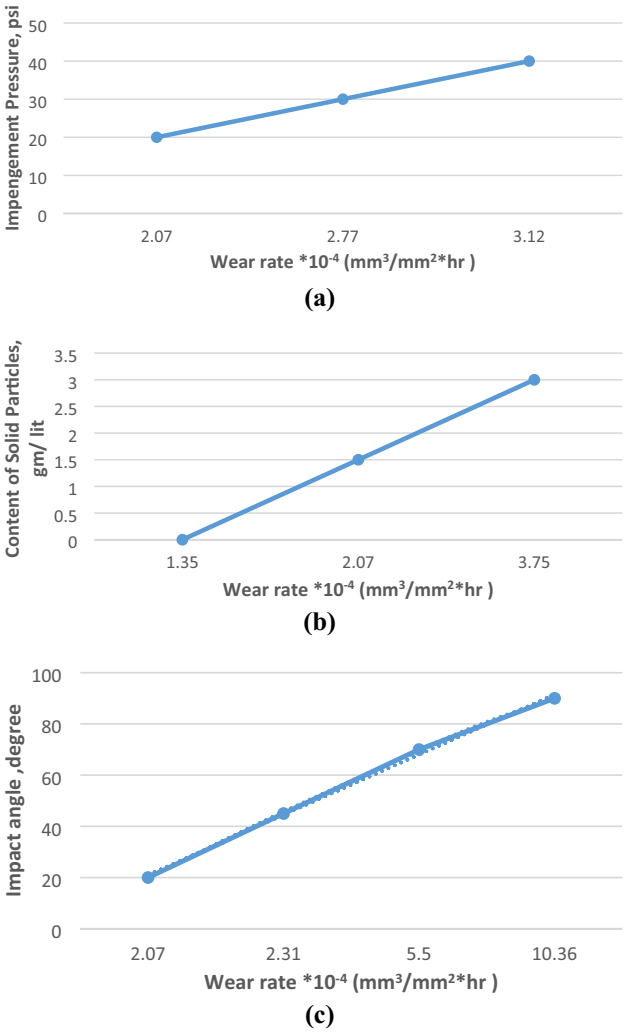

Fig. 11 The statistical analysis of all factors against wear rate **a** Impingement Pressure, **b** content of solid particles, and **c** impact angle degree

increasing the impact angle. At an impact angle of 90°, the total synergism (*S*), based on the E–C's rate, is calculated to be ~ 2.3 times the sum of the material loss because of pure erosion and pure corrosion, separately. The contribution% of erosion "E" increased with increasing impingement angle.

Ploughing and metal cutting were the primary erosion mechanisms at low impact angles, according to SEM pictures taken after 4 h. Flattening of ridges and fatigue fracture, microforging, and throwing/extrusion processes are the primary metal removal processes at high impact angles.

The overall potential values are taken versus the silver–silver chloride electrode that was negatively shifted with increasing the exposure time especially in the case of well water. Increasing the sand content in well water caused by significant surface deterioration and a remarkable shift in the OCP towards more negative values (~ − 1000 mV). The variation in the open-circuit potential with exposure time

is quite different based on the presence of chloride ions as well as load of sand.

Acknowledgements This paper is extracted from a Master Thesis to be submitted to the Faculty of Engineering-Cairo University in partial fulfilment of the Master Degree.

Funding No funding was received to assist with the preparation of this manuscript. Non-financial interests: none.

Data Availability Data will be available on reasonable request. The datasets generated during and/or analysed during the current study are available from the corresponding author on reasonable request.

Declarations

Conflict of interest The authors declare that there is no conflict of interest. The authors have no financial or proprietary interests in any material discussed in this article. Non-financial interests: None.

References

1. Ahmad I, Rahuma MN (2013) Corrosion mitigation and inspection strategy for pipeline integrity management: an experience of Sarir Oilfield. In: Corrosion conference and expo, 2013. NACE International
2. Papavinasam S (2000) Corrosion handbook, 2nd edn. Wiley, New York
3. Kermani M, Morshed A (2003) Carbon dioxide corrosion in oil and gas production—a compendium. Corrosion 59:659–683
4. Chun W (2007) Erosion–corrosion mitigation using chemicals. University of Leeds, Leeds
5. Salama MM (2000) Sand production management. J Energy Resour Technol 122:29–33
6. Salama MM (2000) Influence of sand production on the design and operations of piping systems. In: CORROSION, 2000
7. Tronvoll J, Dusseault M, Sanfilippo F, Santarelli F (2001) The tools of sand management. In: SPE annual technical conference and exhibition, 2001
8. Stack M, Abdulrahman G (2010) Mapping erosion–corrosion of carbon steel in oil exploration conditions: some new approaches to characterizing mechanisms and synergies. Tribol Int 43:1268–1277
9. Finnie I (1958) The mechanism of erosion of ductile metals. In: Paper presented at the 3rd US national congress of applied mechanics, 1958
10. Jordan KG (1998) Erosion in multiphase production of oil and gas. In: CORROSION, 1998, San Diego, California. NACE International, p 34
11. Meng HC, Ludema KC (1995) Wear models and predictive equations: their form and content. Wear 181:443–457
12. Bitter JGA (1963) A study of erosion phenomena: Part I. Wear 6:5–21
13. Bitter JGA (1963) A study of erosion phenomena: Part II. Wear 6:169–190
14. Hutchings IM (1987) Wear by particulates. Chem Eng Sci 42:869–878
15. Tilly GP (1979) Erosion caused by impact of solid particles. Treatise Mater Sci Technol 13:287–319
16. Madsen B (1994) Standard guide for determining the amount of synergism between wear and corrosion—ASTM G119-93. In: 1994 Annual book ASTM standard, vol 3. ASTM, pp 507–512
17. ASM International (1999) ASM handbook, properties and selection: irons, steels, and high-performance alloys. ASM International in the US
18. Zhao Y, Zhou F, Yao J, Dong S, Li N (2015) Erosion–corrosion behavior and corrosion resistance of AISI 316 stainless steel inflow jet impingement. Wear 328:464–474
19. Yang Y, Cheng Y (2012) Parametric effects on the erosion–corrosion rate and mechanism of carbon steel pipes in oil sands slurry. Wear 276:141–148
20. Gulbrandsen E, Bilkova K (2006) Solution chemistry effects on corrosion of carbon steels in the presence of CO_2 and acetic acid. In: CORROSION, 2006
21. Asia Pacific Dental Students Association Ajeel (2010) Damaging of steel-oil pipes by erosion and erosion–corrosion phenomena. Iraqi J Mech Mater Eng 10:97–107
22. Malka R, Nešić S, Gulino DA (2007) Erosion–corrosion and synergistic effects in disturbed liquid-particle flow. Wear 262:791–799
23. Rajahram S, Harvey T, Wood R (2009) Erosion–corrosion resistance of engineering materials in various test conditions. Wear 267:244–254
24. Islam MA, Alam T, Farhat ZN, Mohamed A, Alfantazi A (2015) Effect of microstructure on the erosion behavior of carbon steel. Wear 332–333:1080–1089
25. Abedini M, Ghasemi HM (2014) Synergistic erosion–corrosion behavior of Al–brass alloy at various impingement angles. Wear 319:49–55
26. Abd-Elrhman Y, Abouel-Kasem A, Emara K, Ahmed S (2014) Effect of impact angle on slurry erosion behavior and mechanisms of carburized AISI 5117 steel. J Tribol 136:011106
27. Hutchings I (1981) A model for the erosion of metals by spherical particles at normal incidence. Wear 70:269–281
28. Bellman R Jr, Levy A (1981) Erosion mechanism in ductile metals. Wear 70:A1-27
29. Postlethwaite J (1981) Effect of chromate inhibitor on the mechanical and electrochemical components of erosion–corrosion in aqueous slurries of sand. Corrosion 37:1–5
30. Malik J, Toor I, Ahmed W, Gasem Z, Habib M, Ben-Mansour R, Badr H (2014) Investigations on the corrosion-enhanced erosion behavior of carbon steel AISI 1020. Int J Electrochem Sci 9:6765–6780
31. Levy AV (1986) The platelet mechanism of erosion of ductile metals. Wear 108:1–21
32. Shewmon PG (1983) Effects of hardness on the solid particle erosion mechanisms in AISI 1060 steel. Wear 89:291–302
33. Laguna-Camacho J, Marquina-Chávez A, Mendez-Mendez JV, Vite-Torres M, Gallardo-Hernandez EA (2013) Solid particle erosion of AISI 304, 316 and 420 stainless steels. Wear 301:398–405
34. Li H, Liu Y, Wang Y, Ma J, Cai B, Ji R, Zhang Y (2011) Corrosion–erosion wear of N80 carbon steel and 316L stainless steel in saline–quartz slurry. Mater Corros 62:1051–1060
35. Lopez D, Congote J, Cano J, Toro A, Tschiptschin A (2005) Effect of particle velocity and impact angle on the corrosion–erosion of AISI 304 and AISI 420 stainless steels. Wear 259:118–124
36. Xie J, Alpas A, Northwood D (2003) Mechano-electrochemical effect between erosion and corrosion. J Mater Sci 38:4849–4856
37. Xie J, Alpas AT, Northwood DO (2003) The effect of erosion on the electrochemical properties of AISI 1020 steel. J Mater Eng Perform 12:77–86
38. Zhang G, Cheng Y (2009) Electrochemical corrosion of X65 pipe steel in oil/water emulsion. Corros Sci 51:901–907
39. Tang X, Xu L, Cheng Y (2008) Electrochemical corrosion behavior of X-65 steel in the simulated oil–sand slurry. II: synergism of erosion and corrosion. Corros Sci 50:1469–1474

40. Islam MA, Farhat ZN (2015) Mechanical and electrochemical synergism of API X42 pipeline steel during erosion–corrosion. J Bio- Tribo Corros 1:26
41. Abdel-Karim R, Reda Y, Zohdy KM, Abdelfatah A, El-Raghy S (2019) Electrochemical performance of porous Ni–Cu anodes for direct methanol fuel cells. Int J Electrochem Sci 14:3035–3054
42. Abdelfatah A, Reda Y, Abdel-Karim R, El-Raghy SM, Zohdy KM (2020) Electrochemical characterization of electrodeposited Ni–Cu foams and their application as electrodes for supercapacitors. Front Mech Eng 6:35